Ferromagnetism and Nonmetallic Transport of Thin-Film α-FeSi_{2}: A Stabilized Metastable Material

Guixin Cao, D. J. Singh, X.-G. Zhang, German Samolyuk, Liang Qiao, Chad Parish, Ke Jin, Yanwen Zhang, Hangwen Guo, Siwei Tang, Wenbin Wang, Jieyu Yi, Claudia Cantoni, Wolter Siemons, E. Andrew Payzant, Michael Biegalski, T. Z. Ward, David Mandrus, G. M. Stocks, and Zheng Gai

Phys. Rev. Lett. **114**, 147202 — Published 7 April 2015

DOI: 10.1103/PhysRevLett.114.147202

Ferromagnetism and nonmetallic transport of thin-film α–$FeSi_2$: a stabilized metastable material

Guixin Cao[1], D. J. Singh[2], X.-G. Zhang[1], German Samolyuk[2], Liang Qiao[1], Chad Parish[2], Ke Jin[3], Yanwen Zhang[3,2], Hangwen Guo[2], Siwei Tang[1, 3], Wenbin Wang[2], Jieyu Yi[1,3], Claudia Cantoni[2], Wolter Siemons[2], E. Andrew Payzant[1], Michael Biegalski[1], T. Z. Ward[2], David Mandrus[3,2], G.M. Stocks[2], and Zheng Gai [1,*]

[1]*Center for Nanophase Materials Sciences, Oak Ridge National Laboratory, Oak Ridge, TN 37831*
[2]*Materials Science and Technology Division, Oak Ridge National Laboratory, Oak Ridge, TN 37831-6056*
[3]*Department of Materials Science and Engineering, University of Tennessee, Knoxville, TN 37996*

A metastable phase α-$FeSi_2$ was epitaxially stabilized on silicon substrate using pulsed laser deposition. Nonmetallic and ferromagnetic behaviors were tailored on α-$FeSi_2$ (111) thin films, while the bulk material of α-$FeSi_2$ is metallic and nonmagnetic. The transport property of the films renders two different conducting states with a strong crossover at 50 K which is accompanied by an onset of ferromagnetic transition as well as a substantial magnetoresistance. These experimental results are discussed in terms of the unusual electronic structure of α-$FeSi_2$ obtained within density functional calculations and Boltzmann transport calculations with and without strain. Our finding sheds light on achieving ferromagnetic semiconductors through both the structure and doping tailoring, and provides an example of a tailored material with rich functionalities for both basic research and practical applications.

PACS numbers: 75.47.Np, 75.70.Ak, 68.55.-a, 72.80.Ga

* Corresponding author, Email: gaiz@ornl.gov

Transition-metal disilicides have been extensively investigated in bulk and thin film forms for their roles as constituents in microelectronic and optoelectronic devices.[1-5] In contrast to other metallic disilicides, environmentally friendly iron disilicide ($FeSi_2$) is particularly appealing as a material for thermoelectric or optoelectronic devices due to its semiconductor behavior.[3-5] Very recently, it has been theoretically predicted that semiconducting iron disilicide can even become magnetic through a low level of doping.[6] $FeSi_2$ possesses two main phases, i.e. α phase and β phase. While β-$FeSi_2$ is a well-studied room temperature stable orthorhombic phase, α-$FeSi_2$ is a metastable tetragonal phase with the fluorite structure which only exists at temperatures above 950 ^{o}C.[3-5,7-9] During cooling, the high temperature stable α-$FeSi_2$ phase transforms into the β-$FeSi_2$ phase in terms of energy-lowering Jahn-Teller-like distortion, accompanied by a spontaneous metal-semiconductor transition.[10-12] Although impure α phase (nonmagnetic) can only be occasionally obtained via facing-target sputtering,[13] ion implantation,[14] and annealing of few monolayer films of Fe on Si (111) [15,16] and Si (001) [17,18] substrates, it already shows interesting applications as electrodes or interconnecting material, precursors for achieving Si-β heterostructures.[15,19] Physically, the magnetic properties of metastable phases, can be drastically different from those of equilibrium phases.[20,21] Moreover, special heteroepitaxial relationships can induce new property and change of band structure.[2] The stabilization of the pure metastable α phase is not only important for material applications but also for providing a prototypical system to understand the interplay between chemical bonding, the electronic[22] and magnetic properties.[19,20]

Here we report the epitaxially stabilized metastable phase of α-$FeSi_2$ (111) thin films grown on Si (001) substrate (α-$FeSi_2$(111)□Si(001)) via pulsed laser deposition (PLD). New electronic behavior which is in-between that of metals and semiconductors as well as ferromagnetism are tailored in the film although the α-$FeSi_2$ phase is thought to be metallic and nonmagnetic. An unusual transport property with a strong crossover at 50 K was found accompanied by an onset of

ferromagnetism with a first order transition, as well as a substantial magnetoresistance. Density functional theory (DFT) calculations were performed to provide framework for understanding the transport property and to verify the ferromagnetism with a slight excess of Fe in stoichiometry. The stabilizing and tailoring of the metastable metallic phase towards a semiconducting and magnetic phase may open new pathways to potential device applications.

α-$FeSi_2$(111)□Si(001) films were grown in an ultrahigh vacuum PLD system with reflection high-energy electron diffraction (RHEED). The Si (001) substrate was processed until showing sharp RHEED pattern (Fig. 1(a)). The films were grown at 754 °C with laser flux of 1.2 J cm^{-2} at 2 Hz. During the deposition, the RHEED pattern changed rapidly from Si (001) (2×1) to a new set of pattern as shown in Fig. 1(a), then remained the same to the end of the growth. The film thickness of 50 nm was determined using profilometer and AFM. The structural properties were investigated by high-resolution X-ray diffraction (HRXRD) and electron back scatter diffraction (EBSD). The magnetic properties were measured on a Quantum Design magnetic property measurement system (MPMS) under fields up to 7 T. The electrical resistivity measurements were performed using a Quantum Design physical property measurements system (PPMS). The iron stoichiometry was checked using Rutherford backscattering spectrometry (RBS). A value of Fe-rich around 5% was estimated from the RBS results. The RBS concentrations for other films grown at similar growth condition are consistent.

DFT calculations were performed using the generalized gradient approximation of Perdew, Burke and Ernzerhof.[23] These were done with the general potential linearized augmented planewave (LAPW) method,[24] implemented in the WIEN2k code.[25] The calculations were done for strained film without including the substrate. The LAPW sphere radii were 2.25 Bohr and 1.90 Bohr for Fe and Si, respectively. High convergence criterion of $R_{MIN}*K_{MAX} = 8$, where R_{MIN} is the Si sphere radius. This yields an effective value above 9 for Fe. The standard LAPW method with added local orbitals [26] was used, rather than the APW+lo method.[27] With the above

parameter choice using the standard LAPW+lo basis for all momentum channels is more efficient than a mixture. Local orbitals were used both to include the 3*p* semicore state of Fe with the valence states and to relax any linearization errors in the Fe 3*d* states. The spin-orbital coupling of Fe and Si is included in the calculation. The *P*4/*mmm* unit cell contains Fe at (0,0,0) and Si at (1/2,1/2,±*z*), the value of *z* (0.2731) are determined by total energy minimization. With this structure, each Fe is coordinated by eight Si atoms at a distance of 2.364 Å, while each Si has a short bond to a neighboring Si at 2.333 Å, four Fe neighbors at 2.364 Å, four Si neighbors at 2.690 Å, and one elongated bond Si neighbor at 2.807 Å. The electronic potential is approximated by a hybrid atomic-sphere-approximation muffin-tin with cell shape corrections. [28]

Fig.1 (b) shows the room temperature θ-2θ scan of a α-$FeSi_2$(111)□Si(001) film. The (111) peak of α-$FeSi_2$ is the only extra peak observed other than the Si (002) and (004) reflections, evidencing a single crystalline tetragonal α-$FeSi_2$ phase with (111) orientation. To confirm the preferred orientation of (111), and to determine the epitaxial relationship between the film and substrate, an in-plane pole figure scan was conducted across the (202) Bragg peak of Si (001). Fig.1 (c) shows the (102) Bragg peak of the (111)-type domain of the α-$FeSi_2$ film, which indicates that the α-$FeSi_2$ (102) plane is parallel to Si (202) plane. Moreover, the (102) peak was shown in a fourfold symmetry. EBSD investigation reveals a tetragonal structure with two main $FeSi_2$ domains of the film, confirms the high quality epitaxial nature of the films. Side view and top view of the α-$FeSi_2$ with truncated (111) plane are shown in Fig. 1 (d). Each bulk α-$FeSi_2$ unit cell is formed by two Si atoms (grey or red) and one Fe atom (orange), outlined in blue in the side view figure. As the (111) plane is very complicated, for better viewing the (111) unit cell, red balls are used to mark the topmost layer of the (111) surface. The (111) unit cell is outlined with a black rectangle (10.95 Å × 3.8 Å), very close to the Si (001) (3×1) (11.5 Å × 3.84 Å). Based on above results, we proposed a possible epitaxial model in Fig. 1(e) which satisfies the registration of the α-$FeSi_2$ (111) rectangular unit cell to Si (001) (3×1), and the parallel relation between α-$FeSi_2$ (102) and Si (202) planes (marked with the dotted

blue line in Fig. 1 (e)).

The structure of the α-$FeSi_2$(111)□Si(001) film was further studied as a function of temperature (*T*) using XRD (20 K to 300 K). The *T* dependent *d* spacing was obtained from the shift of the $FeSi_2$ (111) peak during cooling (Fig.2 (a)). The continuous evolution of the *d* spacing suggests the absence of structural phase transitions vs *T*. The linear thermal expansion coefficient α, defined as $\alpha = \frac{1}{d} * \frac{\Delta d}{\Delta T}$, is shown in Fig.2 (a). α is almost a constant at high temperature, and then decreases exponentially in a low temperature region, associated with a sign change around 50 K.

Fig.2 (b) shows the temperature dependent conductance of the α-$FeSi_2$(111)□Si(001) film ($\sigma(T)$) under different magnetic fields. For comparison, the counterpart of Si substrate is also shown. It is clearly seen that the conductance of α-$FeSi_2$(111)□Si(001) film gradually decreases with decreasing temperature (nonmetallic behavior), with a different trend as that of Si. Interestingly, the $\sigma(T)$ curves show an obvious slope change around 50 K. This differs drastically from the bulk phase of the material in which conductivity shows no temperature dependence.[9] Furthermore, the conductance of thin film shows magnetic field dependence. The magnetoresistance MR= (R(0)-R(H))/R(H) reaches 15% at 7 T at low temperature as shown in the inset of Fig. 2 (b), the value is well beyond typical anisotropy induced magnetoresistance.

The field-cooled (FC) and field-warmed (FW) magnetization *M(T)* of the $FeSi_2$ (111) film undergoes a ferromagnetic transition at 50 K (Fig.2 (c)). The system has a first order transition indicated by a sharp cusp in magnetization around T_c.. The similar feature exists for both in-plane and out-of plane magnetization, with stronger in-plane signal than that of the out-of plane. The increase of the susceptibility below 10 K attributes to an impurity induced Curie-like paramagnetic contribution. The field dependent magnetization at 5 K is shown in the inset of Fig.2 (c). The magnetization increases rapidly at low fields and saturates around 4 T as expected for a ferromagnetic behavior. The magnetic saturation moment at 5 K is around 0.2 μ_B per

formula unit.

The MR and the coincidence that the sign change of α, crossover of the electronic transport, and magnetic transition at the same temperature of 50 K, are worth further discussing. For the MR behavior, one possible explanation is the coexistence of ferromagnetic and nonmagnetic phases. If the ferromagnetic phase has highly spin polarized transport, similar to manganites or half-metals, a strong MR can be expected. This can be understood based on the calculated band structure. As discussed below in detail, there shows a strong energy dependence of the electronic structure near the Fermi energy, E_F, and in particular an onset of high density of states (DOS) just above E_F. An exchange splitting of this density of states would lead to majority spin transport, reflecting the high density of states electronic structure above the paramagnetic E_F, and the minority spin transport based on the electronic states that occur below E_F in the paramagnetic case.

There have been prior band structure calculations for α-$FeSi_2$, it consists of hybridized *d* bands on top of a Si *sp* band structure.[10,12,29-31] There is a large peak in the electronic DOS just above E_F which derives from a single Fe *d* band (two fold degenerate with spin-orbit), with different calculations differing about the exact position of the onset relative to E_F. The nominal *d* occupancy is eight, as in elemental Fe, implying that Fe is not a dopant in this material. As such, the Fermi energy position is expected to be insensitive to the Fe stoichiometry, although the DOS may broaden due do disorder effects in actual samples.

To understand the abnormal transport and ferromagnetism tailored in our strain stabilized α-$FeSi_2$(111)□Si(001) films, the calculated band structure and DOS for both the paramagnetic and ferromagnetic phase as well as the majority and minority spin states of Fe and substitutional Fe in strained structures for α-$FeSi_2$ using DFT are shown in Fig. 3 (a) and Fig. 3(b). The distinct dip in the DOS consists with a recent work [32]. Importantly, in our calculation the onset of the DOS peak is almost exactly at the Fermi energy, yielding a highly asymmetric DOS around E_F. This peak comes from the flat band around the zone boundary at $k_z = 0$, i.e. the band seen just at E_F along *X*-*M* in Fig. 3 (a). This band has antibonding Fe d_{z^2} – Si *sp* character. The

other band that crosses E_F has $d_{x^2-y^2}$ character. The strongest predicted signature of this strong energy dependence is a large negative thermopower, unusual for a metal. This prediction provides a test of the electronic structure. One may expect two effects from this electronic structure. The first is that if it becomes ferromagnetic, the transport will be substantially spin polarized, which would be reflected in a negative magnetoresistance, as seen in the inset of Fig. 2(b). Secondly, in non-magnetic samples, which have been reported to grow under other conditions, a temperature dependent cross-over in transport may be expected, specifically from a low density of states metal to an effectively higher density of states metal with increasing *T*.

The origin of ferromagnetism of the α-$FeSi_2$ thin films was investigated using the local density approximation of the DFT implemented within the layer-KKR code [33] and CPA [34] to treat substitutional disorder as shown in Fig. 3 (b). The calculations were done using both the experimentally measured strained (a=2.69 Å, c=5.14 Å) and the unstrained (a=2.72 Å, c=5.42 Å) lattice parameters. For the strained lattice, we found that, as a small percentage of Si atoms are substituted by Fe, those Fe atoms maintain a nearly constant moment of 2.38 μ_B per Fe. Meanwhile, the Fe atoms on the Fe sublattice also acquire a small moment proportional to the amount of substitutinal Fe atoms on the Si sublattice, as shown in the bottom panel of Fig.3 (b). When the substitutional Fe concentration reaches 3.3% (or 6.6% excess per Fe atom), the total net moment reaches 0.2 μ_B per unit cell, consistent with the experimental moment (in the inset of Fig.2(c)). The total energy of the ferromagnetic phase is lower than that of the paramagnetic phase by about 8.66 meV per unit cell. For the unstrained lattice, the energies are reversed, with the total energy of the paramagnetic phase is lower by about 7.23 meV per unit cell.

The Fermi surface for E_F and E_F + 0.025 eV within a rigid band model are shown in Fig. 3 (c) and Fig. 3 (d). The topology of the Fermi surfaces dramatically changes on such a low energy scale. For the actual E_F the Fermi surface consists of small compensating pockets. These include a hole surface around the *M* point, an electron sheet and a complex sheet along the Γ-*M* line. This complex sheet forms

connections near but not exactly at the zone boundary as the Fermi energy is raised. The resulting pipes are a quasi-two-dimensional structure and are the origin of the sharp rise in the DOS. This is reminiscent of the structure seen in *p*-type PbTe [35] and, as in that case, it is expected to affect transport properties. Qualitatively, what may be expected is that the effective DOS will increase with *T*, while the Fermi energy will be pushed down. The conductivity at low *T* can be written as $\sigma \propto N(E_F) < v_F^2 > \tau$, for finite *T*, see Ref. [36]. Here τ is an inverse scattering rate, and $(< v_F^2 >)^{1/2}$ is the effective average Fermi velocity in the direction of the conductivity. *σ(T)* comes from the product of a band structure dependent term $N(E_F)$ and the scattering term τ. For the former term, *T* dependence comes from broadening with a derivative of the Fermi function, while the scattering term in general has a complex *T* dependence depending on the scattering mechanism, typically electron-phonon and electron-spin-fluctuation interactions in metals at moderate temperatures. In the present case, both terms are expected to be non-trivial.

In order to examine this further, we performed calculations of transport functions σ/τ (Fig. 4(a)) within Boltzmann transport theory. [36],[37] In a metal, σ/τ has negligible *T* dependence. Here, however, we find a substantial *T* dependence for *c*-axis transport because of the structure in the DOS near E_F. At low *T*, the scattering (τ) will be governed by point defects and is expected to reflect the behavior of a moderate $N(E_F)$, three dimensional metal with disorder. However, as *T* increases, the effective $N(E_F)$ increases as discussed above. Qualitatively this should both open additional scattering channels for phase space reasons and also may lead to additional scattering if the increased $N(E_F)$ brings the system closer to lattice instabilities or magnetism. Although our calculation does not quantify the transport, the nonmetallic and complicated transport behaviors of the thin films are qualitatively understood. It is noted that the resistance decreases with temperature, but in a non-activated manner, as shown in Fig.2(b). We attribute the resistance to extrinsic grain and domain boundary resistance in the film, consistent with the magnetoresistance.

Interestingly, we also find an anisotropic Seebeck coefficient, $S(T)$, that is anomalously large for a metal especially in the *c*-axis direction, as displayed in Fig.

4(b). $S(T)$ is negative (n type) for both in-plane and c-axis transport, but is much larger in magnitude for the c-axis direction. This reflects the d_{z^2} character of the flat band, which leads to a faster relative increase of the conductivity with energy for the c-axis direction (note that at low T according to the Mott formula $S(T)/T \propto (d\sigma/dE)/\sigma$). Overall, $S(T)$ is more anisotropic than σ/τ, which is also unusual [38] and will be confirmed by further experiments.

In summary, the unusual transport behavior and a temperature dependent cross-over in transport and magnetic properties of α-$FeSi_2$ (111) thin films were tailored by both strain stabilization and substitutional Fe atoms on the Si sublattice. The results were explained based on the fine details of the electronic structure, the stoichiometry, and the strained structure of the film. The material provides an example of a stabilized pure phase with rather interesting physical properties for both basic scientific research and practical applications in for example achieving ferromagnetic semiconductors.

Acknowledgments

This research was conducted at the Center for Nanophase Materials Sciences, which is sponsored at Oak Ridge National Laboratory by the Scientific User Facilities Division, Office of Basic Energy Sciences (ZG, GC, XGZ, LQ, MB, EAP), U.S. Department of Energy. Part of this effort was supported by the U.S. DOE, Office of Basic Energy Sciences, Materials Sciences and Engineering Division, (DS, GS, TZW, GMS, YZ, CP) and under U.S. DOE grant DE-SC0002136 (HWG, WW).

REFERENCES

[1] D. Shah, D. Berczik, D. Anton, and R. Hecht, Materials Science and Engineering: A **155**, 45 (1992).

[2] K. Yamaguchi and K. Mizushima, Physical review letters **86**, 6006 (2001).

[3] D. Leong, M. Harry, K. Reeson, and K. Homewood, Nature **387**, 686 (1997).

[4] B. Egert and G. Panzner, Physical Review B **29**, 2091 (1984).

[5] M. Seibt, R. Khalil, V. Kveder, and W. Schröter, Applied Physics A **96**, 235 (2009).

[6] D. J. Singh and D. Parker, Scientific reports **3** (2013).

[7] A. Cullis and L. Katz, Philosophical Magazine **30**, 1419 (1974).

[8] C. Kloc, E. Arushanov, M. Wendl, H. Hohl, U. Malang, and E. Bucher, Journal of Alloys and Compounds **219**, 93 (1995).

[9] T. Hirano and M. Kaise, Journal of Applied Physics **68**, 627 (1990).

[10] R. Girlanda, E. Piparo, and A. Balzarotti, Journal of applied physics **76**, 2837 (1994).

[11] N. Christensen, Physical Review B **42**, 7148 (1990).

[12] S. Eisebitt, J.-E. Rubensson, M. Nicodemus, T. Böske, S. Blügel, W. Eberhardt, K. Radermacher, S. Mantl, and G. Bihlmayer, Physical Review B **50**, 18330 (1994).

[13] S. Pan, C. Ye, X. Teng, H. Fan, and G. Li, physica status solidi (a) **204**, 3316 (2007).

[14] X. Lin, M. Behar, J. Desimoni, H. Bernas, J. Washburn, and Z. Liliental‐Weber, Applied physics letters **63**, 105 (1993).

[15] N. Jedrecy, A. Waldhauer, M. Sauvage-Simkin, R. Pinchaux, and Y. Zheng, Physical Review B **49**, 4725 (1994).

[16] J. Chevrier, P. Stocker, J. Gay, and J. Derrien, EPL (Europhysics Letters) **22**, 449 (1993).

[17] F. Maeda, H. Hibino, S. Suzuki, and F. Z. Guo, Surface and Interface Analysis **40**, 1747 (2008).

[18] C. Detavernier, C. Lavoie, J. Jordan-Sweet, and A. Özcan, Physical Review B **69**, 174106 (2004).

[19] J. Tripathi, M. Garbrecht, W. Kaplan, G. Markovich, and I. Goldfarb, Nanotechnology **23**, 495603 (2012).

[20] J. Shen, Z. Gai, and J. Kirschner, Surface science reports **52**, 163 (2004).

[21] M. van Schilfgaarde, I. Abrikosov, and B. Johansson, Nature **400**, 46 (1999).

[22] J. Haeni *et al.*, Nature **430**, 758 (2004).

[23] J. Perdew, K. Burke, and M. Ernzerhof, Physical Review Letters **77**, 3865 (1996).

[24] L. Nordstrom and D. J. Singh, *Planewaves, Pseudopotentials, and the LAPW method* (Springer, 2006).

[25] P. Blaha, K. Schwarz, G. Madsen, D. Kvasnicka, and J. Luitz, *WIEN2k: An Augmented Plane Wave plus Local Orbitals Program for Calculating Crystal Properties* (Vienna University of Technology, Austria, 2001).

[26] D. Singh, Physical Review B **43**, 6388 (1991).

[27] E. Sjöstedt, L. Nordström, and D. Singh, Solid state communications **114**, 15 (2000).

[28] X.-G. Zhang and D. Nicholson, Physical review B **60**, 4551 (1999).

[29] J. Van Ek, P. Turchi, and P. Sterne, Physical Review B **54**, 7897 (1996).

[30] Y. Imai, M. Mukaida, and T. Tsunoda, Intermetallics **8**, 381 (2000).

[31] Y. Imai, M. Mukaida, and T. Tsunoda, Thin Solid Films **381**, 176 (2001).

[32] W. Miiller, J. Tomczak, J. Simonson, G. Smith, G. Kotliar, and M. Aronson, arXiv preprint arXiv:1408.3606 (2014).

[33] J. MacLaren, S. Crampin, D. Vvedensky, and J. Pendry, Physical Review B **40**, 12164 (1989).
[34] J. Faulkner and G. Stocks, Physical Review B **21**, 3222 (1980).
[35] D. Parker, X. Chen, and D. J. Singh, Physical Review Letters **110**, 146601 (2013).
[36] G. K. Madsen, K. Schwarz, P. Blaha, and D. J. Singh, Physical Review B **68**, 125212 (2003).
[37] G. K. H. Madsen and D. J. Singh, Computer Physics Communications **175**, 67 (2006).
[38] K. P. Ong, D. J. Singh, and P. Wu, Physical review letters **104**, 176601 (2010).

Figure captions:

FIG. 1 (Color online). (a) The RHEED patterns recorded before and after the growth of α-$FeSi_2$(111)□Si(001). (b) HRXRD (θ-2θ) scan of the film. (**c**) The pole figure at Si (202) plane. (d) Side view and top view of the α-$FeSi_2$ with (111) plane truncated. (e) The epitaxial relation model between the α-$FeSi_2$ and Si (001) (3×1).

FIG. 2 (Color online). (a) Temperature dependent *d* spacing of (111) reflection (left y-axis) and calculated α (right y-axis). The red line is the polynomial fit to the experimental *d* spacing. α crosses zero around 50 K. (b) $\sigma(T)$ for 50 nm α-$FeSi_2$ (111) films under different fields and $\sigma(T)$ of Si (001). Inset shows the MR. (c) $M(T)$ curves under 2 T. The inset shows a typical $M(H)$ loop at 5 K. The dotted line around 50 K is an eye guide for the 50 K transitions.

FIG. 3 (Color online). (a) Calculated band structure of α-$FeSi_2$, including spin-orbit interaction. (b) Top panel: Total DOS for paramagnetic and ferromagnetic phases with the Si sites containing 3.3% substitutional Fe. Bottom panel: Majority and minority spin states of Fe and substitutional Fe in strained structures, respectively. (c) and (d): Fermi surface of α-$FeSi_2$ with E_F and E_F + 0.025 eV. In these plots Γ is at the center.

FIG. 4 (Color online). (a) σ/τ (arbitrary units) vs *T*. (b) $S(T)$ of α-$FeSi_2$ within the constant scattering time approximation.

Fig.1 Cao *et al.*

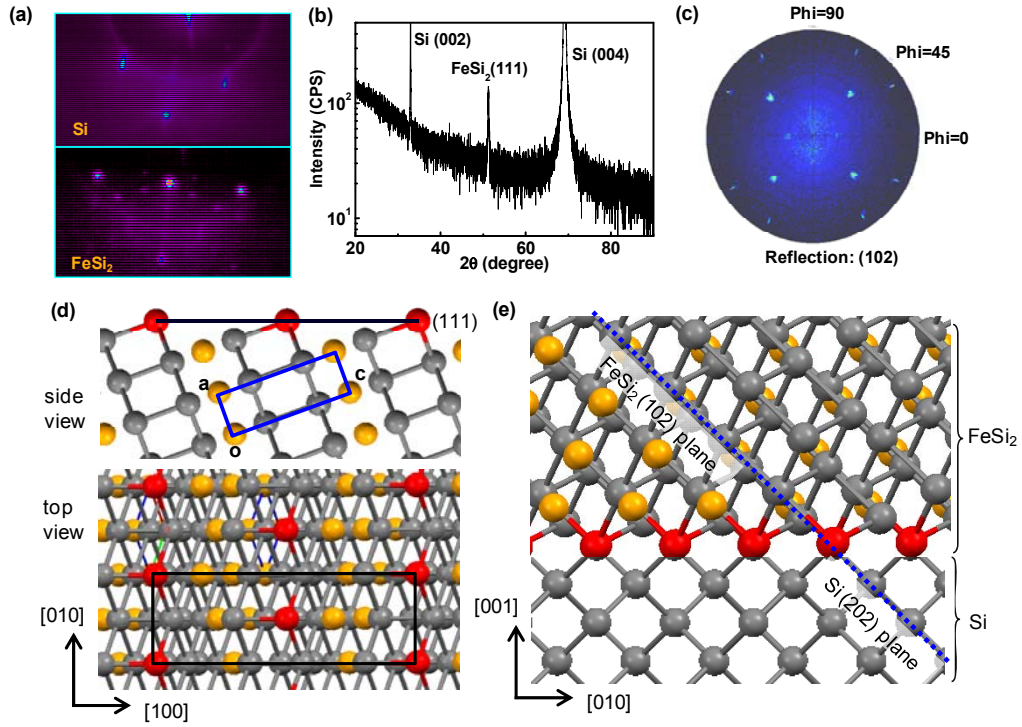

Fig.2 Cao *et al.*

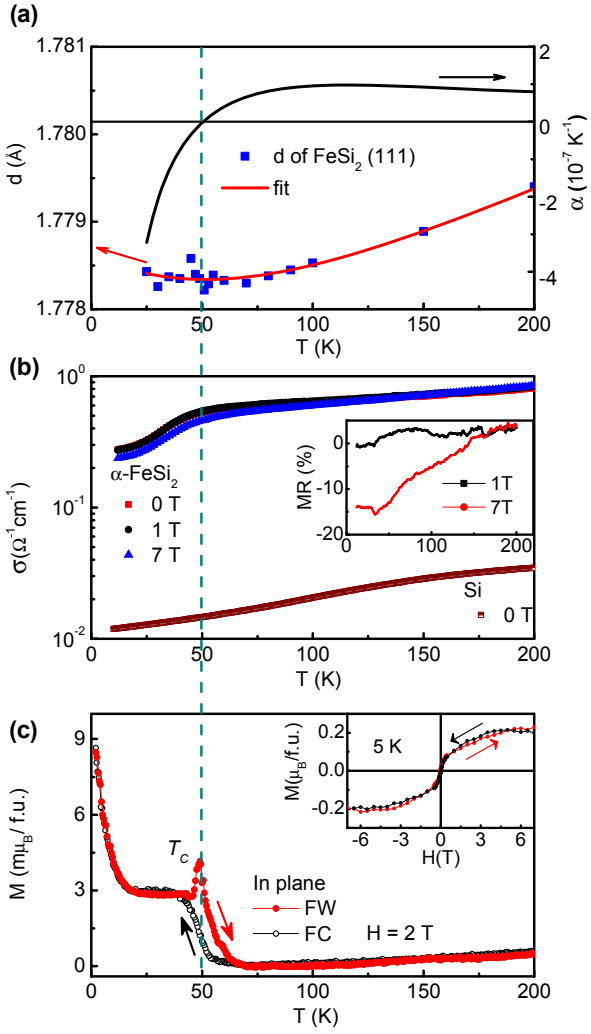

Fig. 3 Cao *et al.*

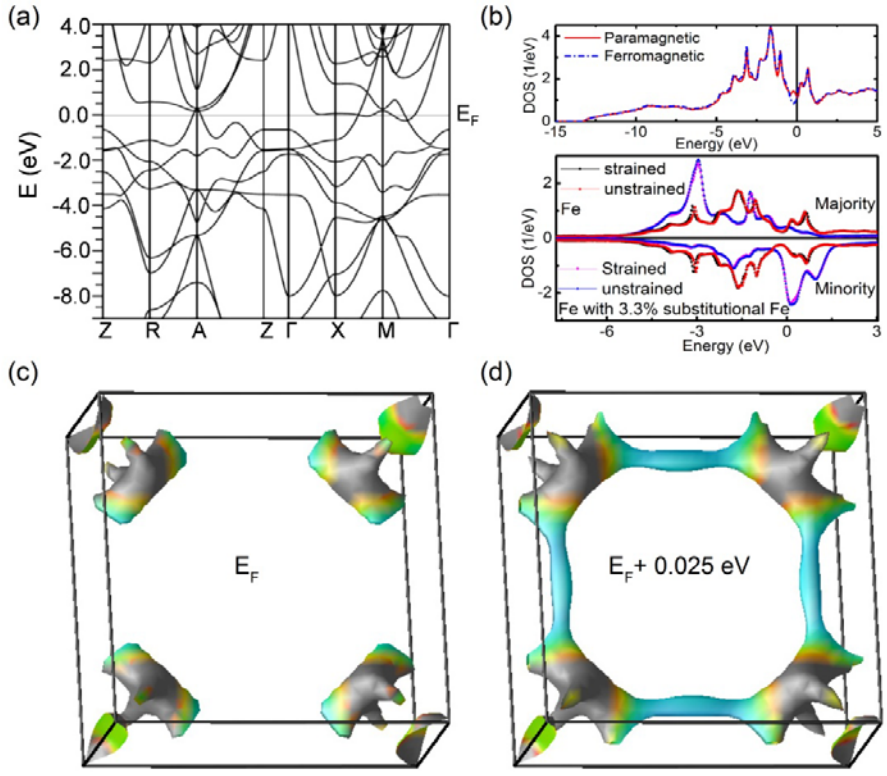

Fig. 4 Cao *et al.*